Programming of the respiratory epithelium *in utero* - insights from the amniotic epithelial methylome

Patricia Agudelo-Romero[1,2,3*†], Thomas Iosifidis[1,4,5,*†], James Lim[1], Nina Kresoje[1], David G. Hancock[1,6,7], Guicheng Zhang[1,4], Abhinav Sharma[8], Talya Conradie[1], Minda Amin[1],Yuliya V. Karpievitch[1,4,9], Desiree T. Silva[7,10,11,12], Anthony Bosco[13,14,] Susan L. Prescott[7,10,15,16], Peter N. LeSouëf [1,17], Elizabeth Kicic-Starcevich[1], Anthony Kicic[1,5,18,19], David J. Martino[1,9,#], Stephen M. Stick[6,#] .

[*]co-first authors, [#]co-senior authors, [†]corresponding authors

Affiliations:

1: Wal-yan Respiratory Research Centre, The Kids Research Institute Australia, Perth, 6009, Western Australia, Australia.

2: School of Molecular Sciences, The University of Western Australia, Perth, Western Australia 6009, Australia.

3: European Virus Bioinformatics Centre, Friedrich-Schiller-Universitat Jena, 07737 Jena, Germany.

4: School of Population Health, Curtin University, Perth, 6102, Western Australia, Australia.

5: Centre for Cell Therapy and Regenerative Medicine, School of Medicine and Pharmacology, The University of Western Australia, Perth, 6009, Western Australia, Australia.

6: Department of Respiratory and Sleep Medicine, Perth Children's Hospital Perth, Perth, 6009, Western Australia, Australia.

7: Medical School, The University of Western Australia, Perth, 6009, Western Australia, Australia.

8: DSI-NRF Centre of Excellence for Biomedical Tuberculosis Research, SAMRC Centre for Tuberculosis Research, Division of Molecular Biology and Human Genetics, Faculty of Medicine and Health Sciences, Stellenbosch University, Cape Town, 7700, South Africa.

9: School of Biomedical Sciences, The University of Western Australia, Perth, 6009, Western Australia, Australia.

10: The Kids Research Institute Australia, Perth, 6009, Western Australia, Australia.

11: School of Medical and Health Sciences, Edith Cowan University, Perth, 6027, Western Australia, Australia.

12: Department of Paediatrics and Neonatology, Joondalup Health Campus, Perth, 6027, Western Australia, Australia.

13: Asthma and Airway Disease Research Center University of Arizona, Tucson, 85721, Arizona, United States.

14: Department of Immunobiology, The University of Arizona College of Medicine, Tucson, 85721, Arizona, United States.

15: Nova Institute for Health, Baltimore, 21231, Maryland, United States.

16: Department of Family and Community Medicine, University of Maryland, Baltimore, 21231, Maryland, United States.

17: School of Paediatrics and Child Health, University of Western Australia, Perth, 6027, Western Australia, Australia.

18: Occupation, Environment and Safety, School of Population Health, Curtin University, Perth, 6102, Western Australia, Australia.

19: Department of Respiratory and Sleep Medicine, Perth Children's Hospital, Perth, 6009, Western Australia, Australia.

***Co-first authors**

[#]**Co-senior authors**

[†]**Correspondence:**

To whom correspondence should be addressed:

Dr Patricia Agudelo-Romero: The Kids Research Institute Australia, Perth Children's Hospital, 15 Hospital Avenue, Nedlands, Western Australia, 6009; Email: Patricia.AgudeloRomero@thekids.org.au

Dr Thomas Iosifidis: The Kids Research Institute Australia, Perth Children's Hospital, 15 Hospital Avenue, Nedlands, Western Australia, 6009; Email: Thomas.Iosifidis@thekids.org.au

Sources of support

This work was supported by grants from the National Health and Medical Research Council of Australia (APP1157548), Department of Health (Western Australia)-Future Health Research and Innovation Fund (2020, 2021, 2022). S.M.S. is supported by an NHMRC Investigator Grant (NHMRC2007725). P.A-R. received funding from the Google Cloud Education Program, a Telethon Kids Institute Theme Collaboration Award grant (PR030564), the Branchi Family Foundation, and a Future Health Research and Innovation (FHRI) Fellowship by the Department of Health (IF2024-25/1), Government of Western Australia. T.I. is supported through the Channel 7 Telethon Trust, Stan Perron Charitable Foundation People Fellowship and previously supported by the Future Health Research Innovation Fund (FHRIF 2020-2023) and Imogen Miranda Suleski Fellowship. A.K is a Rothwell Family Fellow and D.G.H. is a Stan Perron/Perth Children's Hospital Foundation (PCHF) Fellow. D.M. is supported by FHRIF. A.B. is supported by the NIH (R21 AI176305-01A1, R01AI099108-11A1, R01HL132523). The ORIGINS birth cohort has received core funding support from the Paul Ramsay Foundation and the Commonwealth Government of Australia through the Channel 7 Telethon Trust. Substantial in-kind support has been provided by The Kids Research Institute Australia and Joondalup Health Campus.

Running title

Amnion as a surrogate for the newborn airway epithelium

Subject Category

1.12 Clinical asthma
1.17 Epidemiology (Pediatric): Risk Factors < PEDIATRICS
3.40 Airway epithelium < CELL AND MOLECULAR BIOLOGY
3.05 Epigenetics < CELL AND MOLECULAR BIOLOGY
3.02 Bioinformatics/Biological Computing < CELL AND MOLECULAR BIOLOGY

Keywords: Epithelium; airway; amnion; in-utero; exposures; epigenetics; asthma; smoking; DNA methylation; EWAS.

Conflict of Interest declaration: A.B. is a co-founder, equity holder, and director of the startup company Respiradigm Pty Ltd that is related to this work. A.B. is the founder of the startup company INSiGENe Pty Ltd that is related to this work. All other the authors declare that they have no affiliations with or involvement in any organization or entity with any financial interest in the subject matter or materials discussed in this manuscript.

Abstract

Background: Dysregulation of the airway epithelium contributes to recurrent wheezing and asthma and may have developmental origins. Direct interrogation of fetal airway epithelium is not feasible in humans limiting investigation of prenatal epithelial programming.

Methods: We performed high-throughput target-capture DNA methylation sequencing of matched amniotic epithelial biopsies and neonatal nasal brushings from 84 mother-infant pairs within the Airway Epithelium Respiratory Illnesses and Allergy (AERIAL) cohort. We compared tissue-specific methylation landscapes for conservation and explored associations with gestational exposures known to influence childhood asthma risk (maternal asthma history and maternal prenatal smoking exposure).

Results: Between amniotic and nasal tissues, we identified 4,897 differentially methylated regions (FDR $\leq$ 0.05 and $\log_2$FC $\geq$ |0.2|) that were generally hypermethylated in the nasal epithelium. Despite these extensive tissue-specific differences, filtering for non-significant differential methylation loci (FDR $\geq$ 0.1) revealed 1,493,975 CpG loci (~20%) with highly concordant methylation levels between tissues (Pearson's R > 0.8). Within this conserved methylome fraction, we identified exposure-associated CpG sites linked to maternal asthma history (55 CpGs) and prenatal smoking exposure (164 CpGs) that showed consistent directionality in both tissues. These analyses were exploratory and limited by small numbers of exposed participants.

Conclusions: Amniotic epithelium shares a subset of conserved methylation features with the nasal epithelium, supporting its utility as a valuable surrogate for studying aspects of developmental programming of airway vulnerability. While exposure-associated signals were detectable within the conserved methylome fraction, these findings should be considered preliminary, but provide an encouraging framework for early risk stratification in asthma.

121 **Introduction**

122 Asthma is a chronic inflammatory airway disease, among the most frequent causes of
123 hospital admissions in children and represents a significant global disease burden (1–3). A
124 substantial body of evidence suggests prenatal exposures play a critical role in shaping newborn
125 lung function (4), and contribute to the airway epithelial cell dysfunction observed in children
126 with asthma (5). Intrauterine exposure to air pollution and tobacco smoke are well-established risk
127 factors for childhood asthma that impair fetal lung development and increase airway
128 hyperresponsiveness in offspring (6). Similarly, poorly controlled maternal asthma in pregnancy
129 has been associated with childhood wheeze and increased risk for asthma in offspring through
130 alterations in fetal development (7). Animal models also suggest intrauterine chronic inflammatory
131 conditions might directly influence fetal-placental development (8) and aberrant prenatal
132 programming of the airway epithelium tissues (9). Understanding these developmental
133 programming mechanisms is a research priority needed to facilitate early detection and targeted
134 interventions.

135 Epigenetic factors such as DNA methylation play a crucial role in fetal lung development,
136 and changes in DNA methylation have been observed in the airway epithelium in children with
137 asthma (10, 11). Environmental exposures such as cigarette smoke and pollution induce reversible
138 epigenetic changes in airway epithelial cells via oxidative stress (12, 13), disrupting developmental
139 gene expression patterns, and contributing to asthma development (14, 15). Methylation may
140 therefore be an important epigenetic mechanism through which to understand the complex
141 interplay between the prenatal environment and fetal epithelial programming in the development
142 of childhood asthma.

143 A key challenge to studying the prenatal origins of epithelial dysfunction relates to the
144 challenges of sampling the newborn airway epithelial cells, which are difficult to obtain before
145 key postnatal events occur, such as colonization of the mucosal surfaces, and exposure to airborne
146 antigens. To address this, we explored the utility of fetal amniotic epithelial tissue as a surrogate
147 for airway epithelial cells (16). The amnion is exposed to the maternal environment and may harbor
148 epigenetic signatures (17, 18) that reflect processes occurring in the developing fetal respiratory
149 tract. Amniotic epithelial cells possess stem cell like characteristics and are also attractive targets
150 for cellular therapy (19). In this observational study, we explored the landscape of DNA
151 methylation in amniotic epithelium and matched nasal epithelial samples from a cohort of healthy
152 term newborns from the Airway Epithelium Respiratory Illnesses and Allergy (AERIAL) study
153 (20). We conducted a comparative analysis of genome-wide DNA methylation profiles and
154 examined the relative conservation of DNA methylation patterning at specific genes crucial for
155 lung and epithelial development. We also explored whether methylation changes associations with
156 key maternal exposures that influence asthma development were conserved in both tissues. Our
157 results inform ongoing developmental programming studies on epithelium vulnerability.

158 **Methods**

159 **Study design and samples**

160 AERIAL (20) is a substudy nested within the ORIGINS birth cohort (21, 22). Matched newborn
161 amnion biopsies, nasal epithelial brushings, and maternal urine were collected from 84 mother–
162 infant pairs. Maternal asthma history and prenatal tobacco-smoke exposure were ascertained from
163 at least two consecutive questionnaires administered at 20, 28, and 36 weeks' gestation. The study
164 was approved by the Ramsey Health Care HREC WA-SA (#1908) and written informed consent
165 was obtained.

166 **Sample processing and DNA extraction**

167 Placentas were processed within 48 hours after delivery (mean 20.4 ± 13.1 hours [SD]);
168 with the chorion membrane manually separated (23) and amnion sampled. Newborn nasal
169 brushings were collected within 6 weeks from birth (15.9 ± 7.9 days [SD]) (20). Samples were
170 cryopreserved at −80°C. Genomic DNA was extracted from both tissues using the Chemagic 360
171 automated nucleic acid isolation system (Revvity, Baesweiler, Germany) and the Chemagic™
172 DNA Blood 400 Kit H96 (Revvity, part# CMG-1091), and quantified by fluorometry using the
173 Qubit HS dsDNA Assay (Q32854, Thermo Fisher Scientific) (Figure E1 in the online supplement).

174 **Targeted DNA methylation sequencing**

175 Targeted DNA methylation profiling was performed using enzymatic methyl-seq (EM-seq) with
176 capture enrichment (TWIST Human Methylome Panel). Libraries were prepared from 200 ng
177 genomic DNA, pooled pre-capture, enriched by hybridization capture, PCR amplified, and
178 sequenced on an Illumina NovaSeq 6000 (paired-end 150 bp) (Figure E1 in the online supplement).

179 **Bioinformatics**

180 FASTQ files were processed using nf-core/methylseq v23.04.2 (24) and aligned to GRCh38 with
181 BWA-meth; methylation was called with MethylDackel and QC metrics generated using target-
182 methylseq-qc v2.1.0 (25). Panel-specific interval filtering was applied prior to downstream
183 analyses (Supplemental Methods; Figure E1). Analyses used ABLeS (26) and Pawsey resources
184 (27, 28). Scripts are available at https://github.com/wal-
185 yan/AERIAL/tree/main/RespEpithelium_Methylome.

186 **Statistical analysis**

187 Analyses were performed in R v4.3.2 (RStudio v2023.03.0+386) (29) (Supplemental Methods;
188 Figure E1). CpGs with zero coverage in any sample, low coverage (<5), or extreme coverage
189 (>500) were removed; mitochondrial and non-standard chromosomes were excluded. Methylation
190 was expressed as β = methylated/(methylated+unmethylated) ×100 and transformed to M values
191 for statistical modelling. Sample QC included sex inference and principal component analysis.
192 Tissue differences were assessed at the region (DMR) and CpG (DMP) levels using Benjamini–
193 Hochberg FDR correction. DMRs were identified using DMRcate v2.16.1 (30) (tissue as primary
194 predictor, adjusted for sex), requiring ≥50 CpGs per region (FDR ≤0.01; |mean difference| ≥1).
195 DMPs were tested using limma v3.58 (31) with sex as a fixed effect and paired samples accounted
196 for using *duplicateCorrelation()* with participant ID (FDR ≤0.05; |log2FC| ≥0.2). Conserved CpGs
197 were defined as non-differential between tissues (FDR ≥0.1) with high concordance (Pearson R
198 ≥0.8). Maternal asthma and in utero smoke exposures were tested at conserved CpGs using limma
199 (adjusted for sex; participant ID block; FDR ≤0.05; |log2FC| ≥0.2). CpGs/regions were annotated
200 to genes, and GO enrichment was assessed using GREAT-based analyses v2.4.0 (32). Cell
201 deconvolution was not performed as validated reference methylomes for amniotic epithelium are

202 not currently available and inclusion of surrogate variables introduced instability in the paired
203 modelling framework.

204 **Urinary cotinine**

205 Maternal smoking was self-reported and validated using urinary cotinine (33) measured at 20 and
206 36 weeks' gestation (21, 22) with the Salimetrics® High Sensitivity Salivary Cotinine Enzyme
207 Immunoassay Kit (Cat No. 1-2002-5; Salimetrics, State College, PA, USA). Cotinine >10 ng/mL
208 indicated active smoking.

209 **Data availability**

210 Raw sequencing data cannot be shared due to ethical/privacy restrictions. De-identified
211 methylation β and M values for participants who provided genomics data sharing consent are
212 deposited in Mendeley Data (https://data.mendeley.com/datasets/xsch4ysfsn/1). De-identified
213 data for these participants are available from the authors upon reasonable request.

214

Results

Demographics and Sequencing quality

The characteristics of the study population are presented in Table 1. While the newborns' ethnic backgrounds were diverse, the cohort was predominantly Caucasian, with 51.2% of mothers and 48.8% of fathers identifying as such. Newborns had a mean gestational age of 39.12 ± 1.28 weeks [SD], with three preterm births recorded in the cohort, occurring between 35 and 36 weeks of gestation. Sequencing quality statistics were similar across tissues (Table 2), with low duplication rates and 93% of bases covered at a depth of at least 30X. The average number of paired-end sequences generated was approximately 183 ± 28.90 [SD] million for amnion samples and 168.67 ± 33.50 [SD] million for nasal samples. The methylation status was assessed across 7,936,546 million individual CpG dinucleotides, with 6,961,516 remaining after quality control filtering. Fold-80 base penalty metrics were between 1.2-1.6 across all samples indicating good uniformity of coverage for low-diversity libraries.

Differential Methylation Landscape Between Amniotic and Nasal Tissues

We began by examining the general features of epithelium methylation landscapes between amniotic and nasal tissues, which revealed similar enrichment of methylated CpG sites around transcriptional start sites (Figure 1A), and the distribution of methylated and unmethylated CpG islands was similar across tissues (Figure 1B). These patterns were consistent across gene promoters and other regulatory features such as gene enhancers (Figure 1A and Figure E2A in the online supplement). Despite the overall similarities in CpG enrichment, dimensional reduction analysis of all 6,961,516 CpG sites across the genome revealed tissue type as the primary source

236 of variation in DNA methylation profiles (PERMANOVA: pseudo-F=91.52, R^2 0.36, p-
237 value=0.001) suggesting substantial tissue-specific differences (Figure 1C).

238 To determine the extent of tissue-specific differences in DNA methylation patterns, we
239 conducted differential analysis comparing amniotic and nasal epithelium at individual CpG sites
240 and identifying the differentially methylated regions (DMR). This analysis revealed 716,075
241 individual CpGs that contributed to 4,897 genome-wide significant DMRs (Table E1 in the online
242 supplement). Notably, in the nasal epithelium most regions exhibited higher methylation, at 3,847
243 regions (78.50%), while 1,050 regions (21.50%) showed a loss in methylation, compared to the
244 amniotic epithelium. The volcano plot highlights the most hypomethylated region in amnion
245 relative to nasal tissue as an intergenic region on chromosome 15 (chr15:70473876-70475721),
246 while the most hypermethylated region was within the *NAXD* gene on chromosome 13
247 (chr13:110626965-110629183) (Figure 2A). Genomic track visualization revealed broad and
248 consistent methylation differences across these loci (Figure 2B). The intergenic region on
249 chromosome 15 exhibited higher methylation levels in amnion, whereas *NAXD* on chromosome
250 13 showed increased methylation in nasal tissue (Figure 2B). To gain broader insights into the
251 biological processes associated with these methylation differences, we annotated DMRs to the
252 nearest genes and performed Gene Ontology (GO) enrichment analysis. This revealed strong
253 enrichment of pathways related to development and differentiation, with additional ontologies
254 related to stimuli and metabolic processes (Figure 2C and Figure E2B in the online supplement).

255 **Conservation of Methylation Across A Subset of Lung Specific Genes**

256 We identified a conserved methylation signature (Figure 3A and Table E2 in the online
257 supplement), comprising 1,493,975 CpG loci, representing approximately 21% of the total CpG

258 landscape (n=6,961,516). This conserved pattern was distributed across all genomic regulatory
259 features, with the highest representation in introns (20.09%), CpG islands (14.10%), and promoters
260 (12.10%) (Figure E2A in the online supplement). To explore whether there are conserved
261 methylation patterns in genes biologically relevant to epithelial and lung development, we queried
262 the Genotype-Tissue Expression (GTEx) consortium database (https://gtexportal.org/home/) to
263 extract a set of genes uniquely expressed in lung tissue compared to all other anatomical sites (total
264 459 genes). Among these gene sets, 159 genes (~34.6%) exhibited highly concordant methylation
265 patterns (Pearson's R ≥ 0.8) between the two tissues and general conservation of the methylation
266 landscape (Figure 3B). For instance, Surfactant Protein A1 (*SFTPA1)* exhibited intermediate levels
267 of DNA methylation in both amnion and nasal tissues (Figure E2B in the online supplement),
268 while the epithelial specific gene, Secretoglobin Family 3A Member 1 (*SCGB3A1),* known to
269 regulate cell proliferation was predominantly hypomethylated in both tissues (Figure E2B in the
270 online supplement), indicating conservation in subsets of biologically relevant genes. We
271 conducted a pathway enrichment analysis of the conserved signature revealing enrichment of terms
272 related to anatomical and morphogenic processes, cellular organization, metabolism and cell
273 cycling, as well as the regulation of signal transduction and stimulus response (Figure 3D and
274 Figure E2C in the online supplement).

275 **Amnion tissue preserves methylation signatures associated with exposures during pregnancy**

276 Within the conserved portion of the methylome (Table E2 in the online supplement), we
277 investigated statistical associations with two well-characterized exposures known to increase the
278 risk of asthma development in offspring: maternal asthma history and *in utero s*moking exposure
279 (34). In this cohort, 9 out of 84 mothers reported a history of asthma. Binary logistic regression
280 analysis, adjusted for multiple comparisons (FDR ≤ 0.05), identified a small but significant

281 associations at 55 CpG sites (51 hypermethylated and 4 hypomethylated) with maternal asthma
282 (Table 3 and Table E3 in the online supplement). Principal component analysis (PCA) of the
283 conserved CpG sites was significantly associated with maternal asthma history and this exposure
284 was the major driver of variation in DNA methylation at these CpGs in both tissues
285 (PERMANOVA: pseudo-F=27.03, R^2 0.14, p-value=0.0001) (Figure 4A). Enrichment analysis
286 linked these DMPs to pathways involved in cellular response to stimulus, organization and
287 development (Figure E3 in the online supplement). We applied Partial Least Squares -
288 Discriminant Analysis (PLS-DA) for assessing the most relevant features, which identified the 15
289 CpGs contributing to group separation including four CpGs annotated to *MTHFSD* (Figure 4B).
290 Consistent with the separation, the most discriminative CpGs showed lower methylation (M-
291 values) in the maternal asthma group, with similar patterns across both tissues. We visualized the
292 top three CpG sites shown in Figure 4C, chr16:86536881 (*MTHFSD*), chr16:86537583
293 (*MTHFSD*), and chr12:22507624 (*C2CD5/C2CD5-AS1*), which exhibited consistent differences
294 in both amnion and nasal tissues in relation to maternal asthma history.

295 Next, we used the urinary cotinine measurements at 20 and 36 weeks of gestation as a
296 marker of intrauterine smoke exposure. In our cohort, 4 of 88 mothers had cotinine levels
297 consistent with tobacco smoking. Binary logistic regression analysis identified 164 CpG
298 significant associations (126 hypermethylated and 38 hypomethylated) with maternal smoking
299 exposure (Table 4 and Table E4 in the online supplement). Principal component analysis (PCA)
300 of the conserved CpG sites significantly associated with smoking exposure identified it as primary
301 source of the variation in DNA methylation in both tissues (PERMANOVA: pseudo-F=27.23, R^2
302 0.15, p-value=0.001) (Figure 5A), with significant enrichment of pathways involved in regulation
303 of localization, cell activation, proliferation, and lung development (Figure E4 in the online

304 supplement). By applying PLS-DA the 15 highly ranked features contributing to group separation
305 (Figure 5B) comprised 14 CpG sites with decreased levels in the exposed group, while one CpG
306 increased. Visualization of the top three significant CpG sites: chr12:116575870 (*MAP1LC3B2*),
307 chr14:74362734, and chr17:36093007 (*CCL3*), also demonstrated the consistency of these changes
308 across both amnion and nasal tissues between individuals with and without prenatal smoking
309 exposure (Figure 5C).

310

311 **Discussion**

312 In this study we evaluated the extent to which amniotic epithelium reflects DNA methylation
313 features of the neonatal nasal airway epithelium, with the goal of assessing its utility for studying
314 fetal programming of epithelial function relevant asthma development. To achieve this, we
315 investigated the relationship between the amniotic and nasal epithelial methylation landscapes in
316 ex vivo samples from newborns from a well characterized cohort. Our data suggest a sizeable
317 fraction of CpG loci shows highly concordant methylation levels across tissues, enriched for genes
318 involved in developmentally relevant pathways suggesting shared regulatory features established
319 in fetal development.

320 Substantial tissue-specific methylation differences existed between the two tissues,
321 characterized by a predominantly hypomethylated profile (reduced methylation) in amniotic
322 epithelium samples. Given that DNA methylation levels typically increase in more terminally
323 differentiated cell types, reflecting a more restrictive chromatin structure, this hypomethylation in
324 amniotic tissue aligns with its more pluripotent state and stem-cell like characteristics reported in
325 regenerative medicine studies (19). Despite these considerable differences, general features of the
326 methylation landscape were similar, including enrichment of methylated CpGs around
327 transcriptional start sites and low methylation across CpG Islands. consistent with patterns reported
328 across multiple human somatic tissues (35). At the same time, histone modifications have been
329 reported to contribute to epithelial plasticity, which is involved in both development and disease
330 progression (36, 37). This divergence in epigenetic control may facilitate tissue-specific
331 adaptations and responses to environmental changes, underscoring the dynamic nature of the
332 epigenome.

333 Around 20% of the regions captured by the EM-seq target capture assay exhibited very
334 high concordance of methylation levels, which we deemed the 'conserved methylome' between
335 amniotic and nasal tissues (Figure 3A, Table E2 in the online supplement). This shared methylation
336 signature may reflect common developmental and regulatory pathways shaped by the established
337 during fetal development. Importantly these conserved loci imply a restricted subset of the
338 methylome that may capture shared developmental or regulatory programs. Amniotic fluid
339 contains bioactive molecules that play essential roles in fetal development, particularly by
340 influencing critical cellular processes in lung epithelial cells (38). Additionally, the amniotic
341 membrane contributes to the production of surfactant proteins and lipids vital for fetal lung
342 maturation (39). Notably, within this conserved fraction, genes that play a critical role in lung
343 development were represented, supporting the utility for amniotic tissue as a window for
344 developmental programming of the respiratory epithelium (Figure 3B). However, the extent to
345 which additional biologically relevant genes and loci fall outside the regions interrogated remains
346 unknown. Additionally, the temporal separation between tissue sampling (up to six-week post-
347 delivery for nasal samples) which reflects practical challenges in cohort studies means we cannot
348 exclude the possibility that some methylation features in the nasal epithelium reflect early postnatal
349 exposures. However this would be expected to reduce cross-tissue concordance, and the stability
350 of the conserved CpG identified may reflect marks established prenatally that persist into the early
351 postnatal period. Future studies using more comprehensive and unbiased methods, such as whole-
352 genome bisulfite sequencing, could help uncover additional loci of interest.

353 Within the conserved methylome fraction, we conduced exploratory analyses to assess
354 whether selected maternal exposures known to influence the development of asthma were reflected
355 in both tissues (Figure 5 and Figure 6). Associations with maternal asthma history and prenatal

356 smoking exposure were identified at a limited number of CpG loci, with directionally consistent
357 effects observed in amniotic and nasal epithelium (Table E3 in the online supplement). These
358 findings suggest that some exposure-related epigenetic signals established in utero may persist
359 within shared epithelial regulatory regions after birth, consistent with previous studies (40, 41).

360 These exposure analyses must be interpreted cautiously. The number of exposed
361 participants was small limiting statistical power and increasing susceptibility to outlier effects. Our
362 exposure testing was intentionally restricted to the conserved methylome fraction, precluding
363 inference regarding tissue-specific exposure effects or overall concordance across the epithelium.
364 We leveraged PLS-DA purely for data visualization and descriptive summaries, not for feature
365 selection or classification. We also acknowledge the observational nature of this study precludes
366 establishing causality. These results are therefore best viewed as hypothesis-generating signals that
367 motivate future studies in larger cohorts.

368 In conclusion, this study demonstrates that amniotic epithelium shares a restricted but
369 biologically meaningful subset of DNA methylation features with the neonatal nasal airway
370 epithelium. These support the use of amniotic tissue as a complimentary tissue to assess aspects
371 of prenatal programming, providing opportunity for early risk stratification when direct sampling
372 of airway epithelial cells from newborns is not feasible. Larger longitudinal studies incorporating
373 clinical respiratory outcomes are planned to further establish the relevance of exposure-associated
374 methylation signals for asthma risk stratification.

375

Acknowledgments

We would like to thank the contributions of the AERIAL families, together with the cohort study investigator Jose A. Caparros-Martin, Lidija Turkovic, and our consumers Rael Rivers, Kate McGee and Olivia Gleeson, and the Western Australian Epithelial Research Program Consumer Reference Group for their contributions towards project inception/design and its adaptation through COVID-19 and other related amendments.

We also extend our gratitude to the hardworking and dedicated AERIAL research team for recruitment, liaising, and sample collection and processing over the duration of this study, with special mention to Bailee Renouf, Courtney Kidd and Ashleigh Heng-Chin.

We are grateful to all the ORIGINS families who support the project. We would also like to acknowledge and thank the following teams and individuals who have made ORIGINS possible: ORIGINS project team; Joondalup Health Campus (JHC); members of ORIGINS Community Reference and Participant Reference Groups; Research Interest Groups and the ORIGINS Scientific Committee; The Kids Research Institute Australia; City of Wanneroo; City of Joondalup; and Professor Fiona Stanley.

This study is a sub-project of ORIGINS. This unique long-term study, a collaboration between The Kids Research Institute Australia and Joondalup Health Campus, is one of the most comprehensive studies of pregnant women and their families in Australia to date, recruiting 10,000 families over a decade from the Joondalup and Wanneroo communities of Western Australia.

References

1. Inoue Y, Shimojo N. Epidemiology of virus-induced wheezing/asthma in children. *Front Microbiol* 2013;4:.
2. Alvarez-Alvarez I, Niu H, Guillen-Grima F, Aguinaga-Ontoso I. Meta-analysis of prevalence of wheezing and recurrent wheezing in infants. *Allergol Immunopathol (Madr)* 2018;46:210–217.
3. Masoli M, Fabian D, Holt S, Beasley R. The global burden of asthma: Executive summary of the GINA Dissemination Committee Report. *Allergy: European Journal of Allergy and Clinical Immunology* 2004;59:469–478.
4. Stick SM, Burton PR, Gurrin L, Sly PD, LeSouëf PN. Effects of maternal smoking during pregnancy and a family history of asthma on respiratory function in newborn infants. *Lancet* 1996;348:1060–1064.
5. Iosifidis T, Sutanto EN, Buckley AG, Coleman L, Gill EE, Lee AH, *et al.* Aberrant cell migration contributes to defective airway epithelial repair in childhood wheeze. *JCI Insight* 2020;5:.
6. Wang B, Chen H, Chan YL, Wang G, Oliver BG. Why Do Intrauterine Exposure to Air Pollution and Cigarette Smoke Increase the Risk of Asthma? *Front Cell Dev Biol* 2020;8:.
7. Clifton VL. Managing asthma in pregnancy: effects on future child health. *Lancet Respir Med* 2019;7:485–486.
8. Clifton VL, Moss TJM, Wooldridge AL, Gatford KL, Liravi B, Kim D, *et al.* Development of an experimental model of maternal allergic asthma during pregnancy. *Journal of Physiology* 2016;594:1311–1325.
9. Zazara DE, Wegmann M, Giannou AD, Hierweger AM, Alawi M, Thiele K, *et al.* A prenatally disrupted airway epithelium orchestrates the fetal origin of asthma in mice. *Journal of Allergy and Clinical Immunology* 2020;145:1641–1654.
10. Stefanowicz D, Hackett TL, Garmaroudi FS, Günther OP, Neumann S, Sutanto EN, *et al.* DNA Methylation Profiles of Airway Epithelial Cells and PBMCs from Healthy, Atopic and Asthmatic Children. *PLoS One* 2012;7:.
11. Reese SE, Xu CJ, den Dekker HT, Lee MK, Sikdar S, Ruiz-Arenas C, *et al.* Epigenome-wide meta-analysis of DNA methylation and childhood asthma. *Journal of Allergy and Clinical Immunology* 2019;143:2062–2074.
12. Knopik VS, MaCcani MA, Francazio S, McGeary JE. The epigenetics of maternal cigarette smoking during pregnancy and effects on child development. *Dev Psychopathol* 2012;24:1377–1390.
13. Nonkovic N, Marceau K, McGeary JE, Ramos AM, Palmer RHC, Heath AC, *et al.* Maternal smoking during pregnancy is associated with DNA methylation in early adolescence: A sibling comparison design. *Dev Psychol* 2024;doi:10.1037/DEV0001747.
14. Cherneva R V., Kostadinov D. Epigenetic Targets for Therapeutic Approaches in COPD and Asthma. Nutrigenomics – Possible or Illusive. *Folia Med (Plovdiv)* 2019;61:358–369.
15. Ordovas-Montanes J, Dwyer DF, Nyquist SK, Buchheit KM, Vukovic M, Deb C, *et al.* Allergic inflammatory memory in human respiratory epithelial progenitor cells. *Nature* 2018;560:649–654.
16. Suzuki M, Maekawa R, Patterson NE, Reynolds DM, Calder BR, Reznik SE, *et al.* Amnion as a surrogate tissue reporter of the effects of maternal preeclampsia on the fetus. *Clin Epigenetics* 2016;8:.

17. Ching T, Song MA, Tiirikainen M, Molnar J, Berry M, Towner D, *et al.* Genome-wide hypermethylation coupled with promoter hypomethylation in the chorioamniotic membranes of early onset pre-eclampsia. *Mol Hum Reprod* 2014;20:885–904.
18. Kim J, Pitlick MM, Christine PJ, Schaefer AR, Saleme C, Comas B, *et al.* Genome-wide analysis of DNA methylation in human amnion. *The Scientific World Journal* 2013;2013:.
19. Miki T. Stem cell characteristics and the therapeutic potential of amniotic epithelial cells. *American Journal of Reproductive Immunology* 2018;80:e13003.
20. Kicic-Starcevich E, Hancock DG, Iosifidis T, Agudelo-Romero P, Caparros-Martin JA, Karpievitch Y V., *et al.* Airway epithelium respiratory illnesses and allergy (AERIAL) birth cohort: study protocol. *Frontiers in Allergy* 2024;5:.
21. D'Vaz N, Kidd C, Miller S, Amin M, Davis JA, Talati Z, *et al.* The ORIGINS Project Biobank: A Collaborative Bio Resource for Investigating the Developmental Origins of Health and Disease. *Int J Environ Res Public Health* 2023;20:.
22. Silva DT, Hagemann E, Davis JA, Gibson LY, Srinivasjois R, Palmer DJ, *et al.* Introducing the ORIGINS project: a community-based interventional birth cohort. *Rev Environ Health* 2020;35:281–293.
23. Magatti M, Caruso M, De Munari S, Vertua E, De D, Manuelpillai U, *et al.* Human Amniotic Membrane-Derived Mesenchymal and Epithelial Cells Exert Different Effects on Monocyte-Derived Dendritic Cell Differentiation and Function. *Cell Transplant* 2015;24:1733–1752.
24. DI Tommaso P, Chatzou M, Floden EW, Barja PP, Palumbo E, Notredame C. Nextflow enables reproducible computational workflows. *Nat Biotechnol* 2017;35:316–319.
25. Sharma A, Conradie T, Martino D, Stick S, Agudelo-Romero P. target-methylseq-qc: a lightweight pipeline for collecting metrics from targeted sequence mapping files. *J Open Source Softw* 2025;10:7608.
26. Gustafsson OJR, Al Bkhetan Z, Francis R, Manos S. *Enabling national step changes in bioinformatics through ABLeS, the Australian BioCommons Leadership Share*. *Zenodo* Melbourne, Australia: 2023. doi:https://doi.org/10.5281/zenodo.10139651.
27. Pawsey Supercomputing Research Centre. *Nimbus Research Cloud*. Perth, Western Australia: 2023. at <https://doi.org/10.48569/v0j3-qd51>.
28. Pawsey Supercomputing Research Centre. *Acacia Object Storage*. Perth, Western Australia: 2023. at <https://doi.org/10.48569/nfe9-a426>.
29. R Core Team. R: A language and environment for statistical computing, R Foundation for Statistical. *R Foundation for Statistical Computing* 2021;at <https://www.r-project.org/>.
30. Peters TJ, Buckley MJ, Chen Y, Smyth GK, Goodnow CC, Clark SJ. Calling differentially methylated regions from whole genome bisulphite sequencing with DMRcate. *Nucleic Acids Res* 2021;49:.
31. Ritchie ME, Phipson B, Wu D, Hu Y, Law CW, Shi W, *et al.* Limma powers differential expression analyses for RNA-sequencing and microarray studies. *Nucleic Acids Res* 2015;43:e47.
32. Gu Z, Hübschmann D. rGREAT: an R/bioconductor package for functional enrichment on genomic regions. *Bioinformatics* 2023;39:.
33. Noakes PS, Thomas R, Lane C, Mori TA, Barden AE, Devadason SG, *et al.* Association of maternal smoking with increased infant oxidative stress at 3 months of age. *Thorax* 2007;62:714–717.

34. Bobolea I, Arismendi E, Valero A, Agustí A. Early Life Origins of Asthma: A Review of Potential Effectors. *J Investig Allergol Clin Immunol* 2019;29:168–179.
35. Lokk K, Modhukur V, Rajashekar B, Märtens K, Mägi R, Kolde R, *et al.* DNA methylome profiling of human tissues identifies global and tissue-specific methylation patterns. *Genome Biol* 2014;15:.
36. Kiesslich T, Pichler M, Neureiter D. Epigenetic control of epithelial-mesenchymal-transition in human cancer. *Mol Clin Oncol* 2013;1:3–11.
37. Yuan S, Natesan R, Sanchez-Rivera FJ, Li J, Bhanu N V., Yamazoe T, *et al.* Global regulation of the histone mark H3K36ME2 underlies epithelial plasticity and metastatic progression. *Cancer Discov* 2020;10:854–871.
38. Li B, Chen X, Ma W, Li N, Chen Q, Liao J, *et al.* An endogenous amniotic fluid-derived 10-amino acid peptide improves lung development and hyperoxia injury. *Transl Pediatr* 2023;12:46–55.
39. Lemke A, Castillo-Sánchez JC, Prodinger F, Ceranic A, Hennerbichler-Lugscheider S, Pérez-Gil J, *et al.* Human amniotic membrane as newly identified source of amniotic fluid pulmonary surfactant. *Sci Rep* 2017;7:.
40. Magnaye KM, Clay SM, Nicodemus-Johnson J, Naughton KA, Huffman J, Altman MC, *et al.* DNA methylation signatures in airway cells from adult children of asthmatic mothers reflect subtypes of severe asthma. *Proc Natl Acad Sci U S A* 2022;119:.
41. Joubert BR, Felix JF, Yousefi P, Bakulski KM, Just AC, Breton C, *et al.* DNA Methylation in Newborns and Maternal Smoking in Pregnancy: Genome-wide Consortium Meta-analysis. *Am J Hum Genet* 2016;98:680–696.

511 **Table 1. Demographic characteristics of the Airway Epithelium Respiratory Illnesses and**

512 **Allergy (AERIAL) study.**

Variables	Categories
Gender	**Female** 50 % (n=42) **Male** 50 % (n=42)
Ethnicity	**Mother** Caucasian (51.2 %) Non-caucasian (48.8 %) **Father** Caucasian (44.1 %) Non-caucasian (55.9 %)
Smoking exposure	**Yes** 4.76 % (n=4) **No** 95.54 % (n=80)
Maternal asthma	**Maternal asthma history** 11.91 % (n=10) **No maternal asthma history** 88.09 % (n=74)
Gestational age (mean ± SD)	39.12 ± 1.28 weeks
Delivery Mode	**Vaginal delivery** 47.62% (n=40) **Caesarean delivery** 47.62% (n=40) ***NA*** 4.76% (n=4)

513 ***SD****: standard deviation;* ***NA***: data not available

514

515 **Table 2. Sequencing statistics for 84 matched samples from neonatal nasal and maternal**

516 **amnion.** Values represent the mean ± standard deviation.

	Nasal samples	Amnion samples
M seq (in million)	168.67 ± 33.50	183 ± 28.90
% GC	27 ± 0.01	27% ± 0.01
% Duplication	15% ± 0.03	18% ± 0.03
Insert Size	225.35 bp ± 21.02	212.95 bp ± 9.98
% Target Bases 10X	99% ± 0.00	99% ± 0.00
% Target Bases 30X	93% ± 5.73	93% ± 8.55

517 bp: base pair

518

519 **Table 3. Top 10 Most Differentially Methylated Positions (DMPs) in Maternal Asthma**

520 **History.**

Position	Symbol*	Log_2FC	Adj. p-value
chr16:89629808	*DPEP1*	3.36	0.03172786
chr16:89629809	*DPEP1*	3.02	0.02803976
chr12:109788572	*TRPV4*	2.99	0.02178272
chr5:72381577		2.88	0.02803976
chr5:72381576		2.85	0.03384522
chr12:109777366	*FAM222A-AS1*	2.85	0.008949334
chr1:25812646	*MTFR1L; SELENON*	-2.43	0.02803976
chr1:25813427	*MTFR1L; SELENON*	-2.47	0.03615935
chr6:166412533	*RPS6KA2*	-2.92	0.04016408
chr6:166412532	*RPS6KA2*	-3.36	0.03419868

521 *CpG sites without a gene symbol may be located in regions with incomplete or less characterized
522 gene annotations.
523

524

525 **Table 4. Top 10 Most Differentially Methylated Positions (DMPs) in Maternal Smoking**

526 **Exposure.**

Position	Symbol*	Log_2FC	Adj. p-value
chr8:143251263	*ZFP41*	4.99	0.02767552
chr6:15500540	*JARID2*	4.77	0.019276332
chr11:17779027	*KCNC1*; LOC107984317	4.74	0.015961482
chr8:143229735		4.73	0.012421924
chr14:74362734		4.66	5.60224E-07
chr7:158796784	*ESYT2*	-4.14	0.0415906
chr6:65566339	*EYS*	-4.20	0.008385907
chr12:31887708	LINC02422	-4.20	0.028869893
chr12:31887707	LINC02422	-4.47	0.011409155
chr10:129774152		-4.84	0.002327469

527 *CpG sites without a gene symbol may be located in regions with incomplete or less characterized
528 gene annotations.
529

530

Figure Legends

Figure 1. Comparative analysis of DNA methylation landscapes in amnion and nasal tissues. (A) Density plot illustrating CpG enrichment around Transcriptional Start Sites (TSSs). (B) Methylation levels of CpG islands with ± 2 kb. CpG islands are rescaled to the same width from Start to End vertical lines. (C) Principal component analysis (PCA) of genome-wide DNA methylation tissue profiles reveals distinct clustering of Amnion (red) and Nasal (blue) samples. Principal Component 1 (PC1) accounts for 39.93% of the variance.

Figure 2. Regions differentially methylated between amniotic and nasal samples are enriched in cell development pathways. (A) Volcano plot displaying differentially methylated regions (DMRs) between amnion and nasal tissues. The x-axis represents the mean methylation difference, and the y-axis represents the $\log_2$-transformed region size. Genes associated with the most significant DMRs are labelled in red. (B) Genomic tracks showing methylation loss or gain in specific regions of Chromosomes 13 (*NAXD*) and 15 (Intergenic region), respectively. CpG islands are marked in green. The line graph summarizes the methylation difference between amnion (red) and nasal (blue) tissues across the region. (C) Gene Ontology (GO) enrichment was calculated using genes near DMRs between amniotic and nasal tissues, followed by a similarity matrix analysis. The similarity heatmap clusters significant GO terms into related Biological Process (BP), with colour intensity representing the significance of enrichment. Similarity of related terms within the same cluster is shown in the heatmap.

Figure 3. Conserved methylation landscapes were enriched in cell differentiation and morphogenesis pathways. (A) Scatter plot comparing DNA methylation levels between amnion and nasal tissues. Each dot represents a genomic region, with its position indicating the methylation level in each tissue. The strong positive correlation (Pearson's $R \geq 0.8$, p-value = 0.000) suggests a high degree of conservation in methylation patterns between these tissues. (B) Heatmap illustrating the expression levels of lung- and epithelial-specific genes across various tissues. Each row represents a gene, and each column represents a tissue. The colour intensity indicates the level of expression, with red representing high expression and blue representing low expression. Data are derived from the GTEx catalogue. (C) Gene Ontology (GO) enrichment was calculated using genes near CpG sites from the conserved methylation signature, followed by a similarity matrix analysis. The similarity heatmap displays GO terms associated with Biological Process (BP), with colour intensity representing the significance of enrichment.

Figure 4. Methylation changes associated with maternal asthma in the conserved signature. (A) Principal Component Analysis (PCA) of DNA methylation variation in newborn amnion and nasal tissues, showing the first two principal components (PC1 and PC2). Samples are coloured based on maternal asthma history, with asthma in orange and non-asthma in blue. (B) Bar plot of loading scores from Dimension 1 (Dim1) of a Partial Least Squares Discriminant Analysis (PLS-DA), highlighting the top 15 differentially methylated CpG sites associated with maternal asthma. (C) Violin plots of the top three CpG sites identified by PLS-DA, showing the distribution of methylation levels (expressed as M-values) at features associated with maternal asthma in newborn amnion and nasal tissues, further stratified by maternal asthma history during pregnancy status.

Figure 5. Methylation changes associated with maternal smoking exposure in the conserved signature. (A) Principal Component Analysis (PCA) of DNA methylation variation in newborn amnion and nasal tissues, showing the first two principal components (PC1 and PC2). Samples are coloured based on maternal smoking exposure, with smoking exposure in orange and non-smoking exposure in blue. (B) Bar plot of loading scores from Dimension 1 (Dim1) of a Partial Least Squares Discriminant Analysis (PLS-DA), highlighting the top 15 differentially methylated CpG sites associated with maternal smoking exposure. (C) Violin plots of the top three CpG sites identified by PLS-DA, showing the distribution of methylation levels (expressed as M-values) at features associated with maternal smoking exposure in newborn amnion and nasal tissues, further stratified by prenatal smoking status.

Online Supplement

Table E1. Tissue-Specific Differentially Methylated Regions (DMRs) and Positions (DMPs). Results of differential methylation analysis comparing amniotic and nasal epithelium.

Table E2. Conserved CpG Methylation Across Lung-Specific Genes. List of 1,493,975 CpG loci showing conserved methylation patterns across tissues, with genomic feature annotations.

Table E3. CpG Sites Associated with Maternal Asthma. Binary logistic regression analysis, adjusted for multiple comparisons (FDR ≤ 0.05), identified significant associations at CpG sites with maternal asthma (MA) and smoking exposure (SE).

Supplemental Material

Supplemental Methods.

Figure E1. Analysis Workflow. This study was conducted in three main phases: Sample processing and sequencing (green), Bioinformatics analysis (blue), and Statistical analysis (pink). The statistical analysis phase was further divided into four key steps: Step 1 – Dimensional reduction using Principal Component Analysis (PCA); Step 2 – Differential methylation analysis at the regional level (differentially methylated regions, DMRs) associated with tissue differences; Step 3 – Differential methylation analysis at the CpG site level (differentially methylated positions, DMPs) associated with tissue differences; Step 4 – Identification of a conserved DMP signature, which was then used to assess associations with gestational exposures (maternal asthma and maternal smoking). MD: Mean Difference; FDR: False Discovery Rate; FC: Fold Change.

Figure E2. Conserved methylation landscape across tissues. (A) Histogram counts of CpGs annotated to genomic features for the conserved methylome. (B) Significantly enriched biological processes within the conserved methylome for CpGs annotate to nearest transcriptional start sites. Point size represents count of number of genes relative to total genes within the pathway (C) Raw sequencing coverage across the SFTPA1 genet coding region (top panel) and the SCGB3A1 coding region. Ticks in red are methylated reads and blue represents unmethylated reads. Height of the grey silhouettes represents sequencing coverage.

Figure E3. Pathway enrichment of maternal asthma history. (A) Significantly enriched biological processes within the conserved methylome for CpGs associated with maternal asthma. Point size represents count of number of genes relative to total genes within the pathway. (B) Gene Ontology (GO) enrichment was calculated using genes near CpG sites from the maternal asthma signature, followed by a similarity matrix analysis. The similarity heatmap displays GO terms associated with Biological Process (BP), with colour intensity representing the significance of enrichment.

Figure E4. Pathway enrichment of maternal smoking exposure. (A) Significantly enriched biological processes within the conserved methylome for CpGs associated with maternal smoking. Point size represents count of number of genes relative to total genes within the pathway. (B) Gene Ontology (GO) enrichment was calculated using genes near CpG sites from the maternal smoking signature, followed by a similarity matrix analysis. The similarity heatmap displays GO terms associated with Biological Process (BP), with colour intensity representing the significance of enrichment.

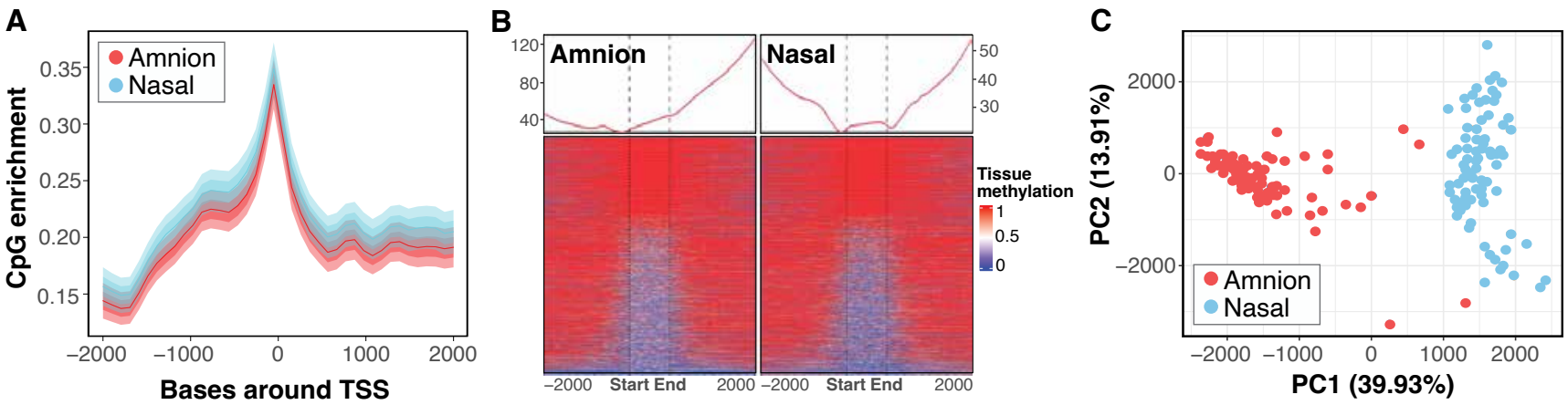

Figure 1. Comparative analysis of DNA methylation landscapes in amnion and nasal tissues. (A) Density plot illustrating CpG enrichment around Transcriptional Start Sites (TSSs). (B) Methylation levels of CpG islands with ± 2 kb. CpG islands are rescaled to the same width from Start to End vertical lines. (C) Principal component analysis (PCA) of genome-wide DNA methylation tissue profiles reveals distinct clustering of Amnion (red) and Nasal (blue) samples. Principal Component 1 (PC1) accounts for 39.93% of the variance.

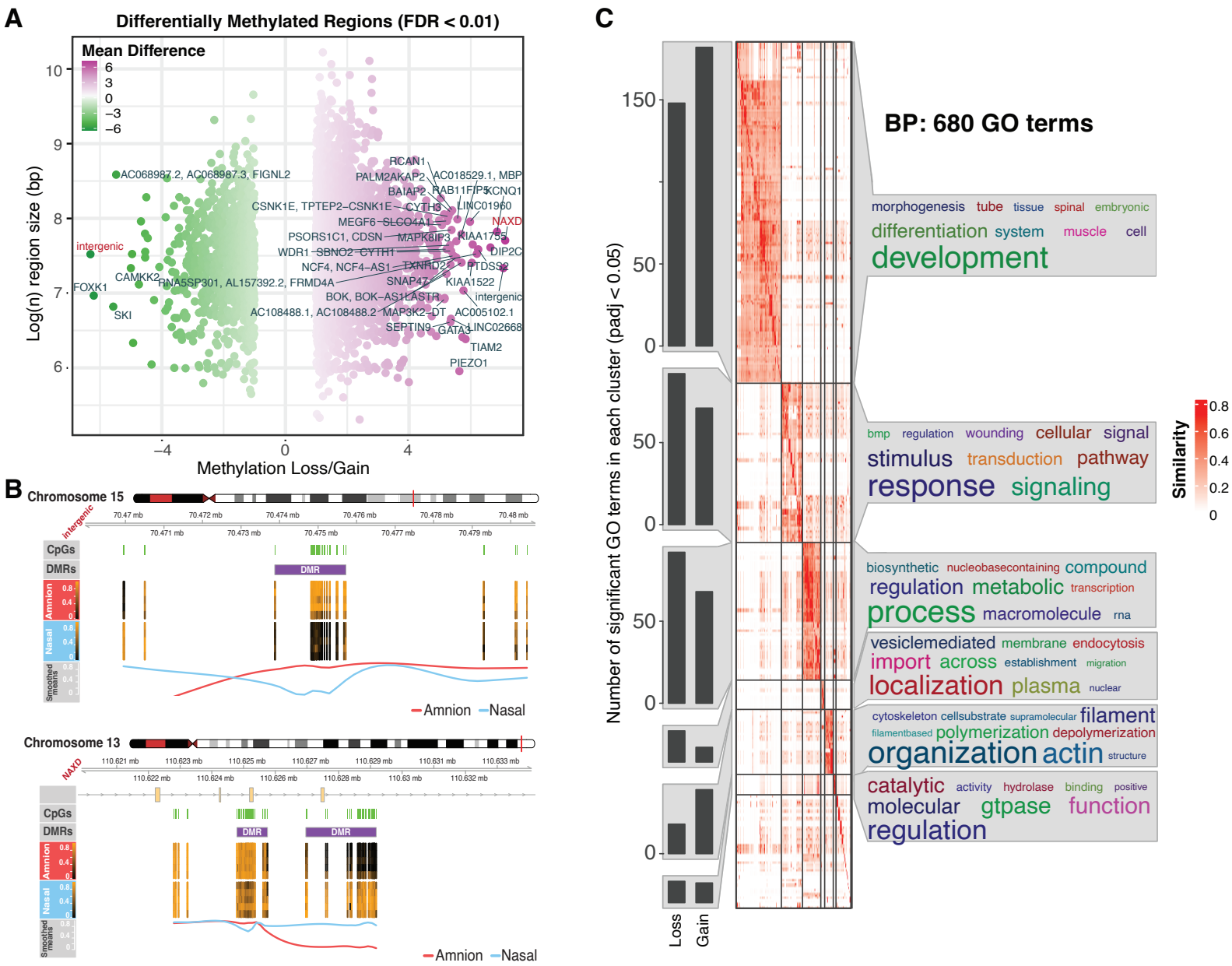
A
Differentially Methylated Regions (FDR < 0.01)
Mean Difference
6
3
0
−3
−6
Log(n) region size (bp)
Methylation Loss/Gain
AC068987.2, AC068987.3, FIGNL2
intergenic
FOXK1
SKI
CAMKK2
RNA5SP301, AL157392.2, FRMD4A
CSNK1E, TPTEP2−CSNK1E
PSORS1C1, CDSN
WDR1
NCF4, NCF4−AS1
BOK, BOK−AS1
AC108488.1, AC108488.2
RCAN1
PALM2AKAP2
AC018529.1, MBP
BAIAP2
RAB11FIP5
KCNQ1
CYTH3
LINC01960
MEGF6
SLCO4A1
NAXD
MAPK8IP3
KIAA1755
DIP2C
TXNRD2
PTDSS2
SNAP47
KIAA1522
LASTR
MAP3K2−DT
AC005102.1
SEPTIN9
GATA3
LINC02668
TIAM2
PIEZO1
B
Chromosome 15
CpGs
DMRs
DMR
Amnion
Nasal
Smoothed means
Amnion
Nasal
Chromosome 13
NAXD
DMR
DMR
C
BP: 680 GO terms
Number of significant GO terms in each cluster (padj < 0.05)
Loss
Gain
morphogenesis tube tissue spinal embryonic
differentiation system muscle cell
development
bmp regulation wounding cellular signal
stimulus transduction pathway
response signaling
biosynthetic nucleobasecontaining compound
regulation metabolic transcription
process macromolecule rna
vesiclemediated membrane endocytosis
import across establishment migration
localization plasma nuclear
cytoskeleton cellsubstrate supramolecular filament
filamentbased polymerization depolymerization
organization actin structure
catalytic activity hydrolase binding positive
molecular gtpase function
regulation
Similarity
0.8
0.6
0.4
0.2
0

645

646 **Figure 2. Regions differentially methylated between amniotic and nasal samples are enriched in cell development pathways.** (A)
647 Volcano plot displaying differentially methylated regions (DMRs) between amnion and nasal tissues. The x-axis represents the mean
648 methylation difference, and the y-axis represents the $\log_2$-transformed region size. Genes associated with the most significant DMRs
649 are labelled in red. (B) Genomic tracks showing methylation loss or gain in specific regions of Chromosomes 13 (*NAXD*) and 15
650 (Intergenic region), respectively. CpG islands are marked in green. The line graph summarizes the methylation difference between
651 amnion (red) and nasal (blue) tissues across the region. (C) Gene Ontology (GO) enrichment was calculated using genes near DMRs
652 between amniotic and nasal tissues, followed by a similarity matrix analysis. The similarity heatmap clusters significant GO terms into
653 related Biological Process (BP), with colour intensity representing the significance of enrichment. Similarity of related terms within the
654 same cluster is shown in the heatmap.
655

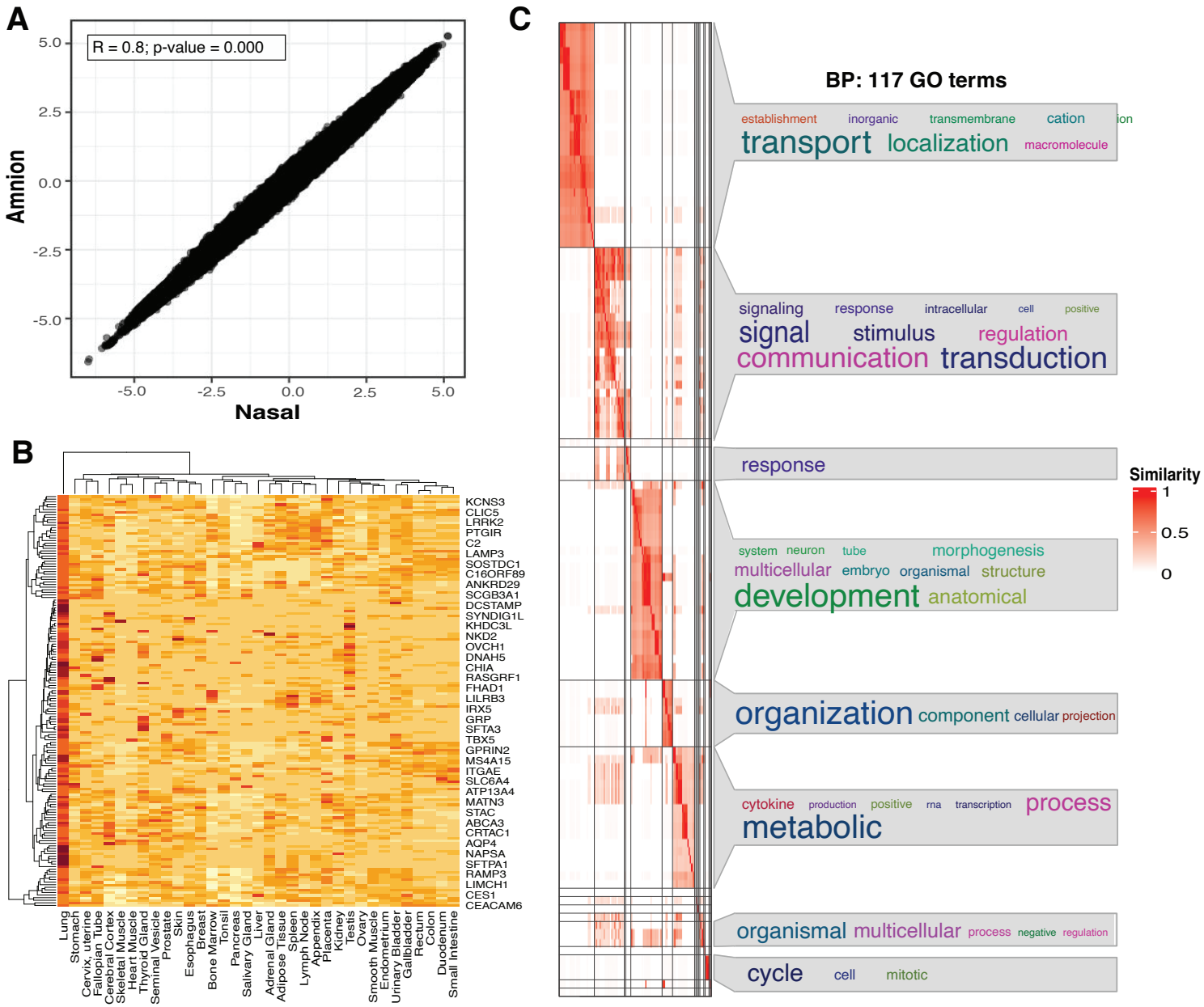
A
R = 0.8; p-value = 0.000
Amnion
Nasal
5.0
2.5
0.0
-2.5
-5.0
B
KCNS3
CLIC5
LRRK2
PTGIR
C2
LAMP3
SOSTDC1
C16ORF89
ANKRD29
SCGB3A1
DCSTAMP
SYNDIG1L
KHDC3L
NKD2
OVCH1
DNAH5
CHIA
RASGRF1
FHAD1
LILRB3
IRX5
GRP
SFTA3
TBX5
GPRIN2
MS4A15
ITGAE
SLC6A4
ATP13A4
MATN3
STAC
ABCA3
CRTAC1
AQP4
NAPSA
SFTPA1
RAMP3
LIMCH1
CES1
CEACAM6
Lung
Stomach
Cervix, uterine
Fallopian Tube
Cerebral Cortex
Skeletal Muscle
Heart Muscle
Thyroid Gland
Seminal Vesicle
Prostate
Skin
Esophagus
Breast
Bone Marrow
Tonsil
Pancreas
Salivary Gland
Liver
Adrenal Gland
Adipose Tissue
Spleen
Lymph Node
Appendix
Placenta
Kidney
Testis
Ovary
Smooth Muscle
Endometrium
Urinary Bladder
Gallbladder
Rectum
Colon
Duodenum
Small Intestine
C
BP: 117 GO terms
establishment inorganic transmembrane cation
transport localization macromolecule
signaling response intracellular cell positive
signal stimulus regulation
communication transduction
response
system neuron tube morphogenesis
multicellular embryo organismal structure
development anatomical
organization component cellular projection
cytokine production positive rna transcription process
metabolic
organismal multicellular process negative regulation
cycle cell mitotic
Similarity
1
0.5
0

656

Figure 3. Conserved methylation landscapes were enriched in cell differentiation and morphogenesis pathways. (A) Scatter plot comparing DNA methylation levels between amnion and nasal tissues. Each dot represents a genomic region, with its position indicating the methylation level in each tissue. The strong positive correlation (Pearson's $R \geq 0.8$, p-value = 0.000) suggests a high degree of conservation in methylation patterns between these tissues. (B) Heatmap illustrating the expression levels of lung- and epithelial-specific genes across various tissues. Each row represents a gene, and each column represents a tissue. The colour intensity indicates the level of expression, with red representing high expression and blue representing low expression. Data are derived from the GTEx catalogue. (C) Gene Ontology (GO) enrichment was calculated using genes near CpG sites from the conserved methylation signature, followed by a similarity matrix analysis. The similarity heatmap displays GO terms associated with Biological Process (BP), with colour intensity representing the significance of enrichment.

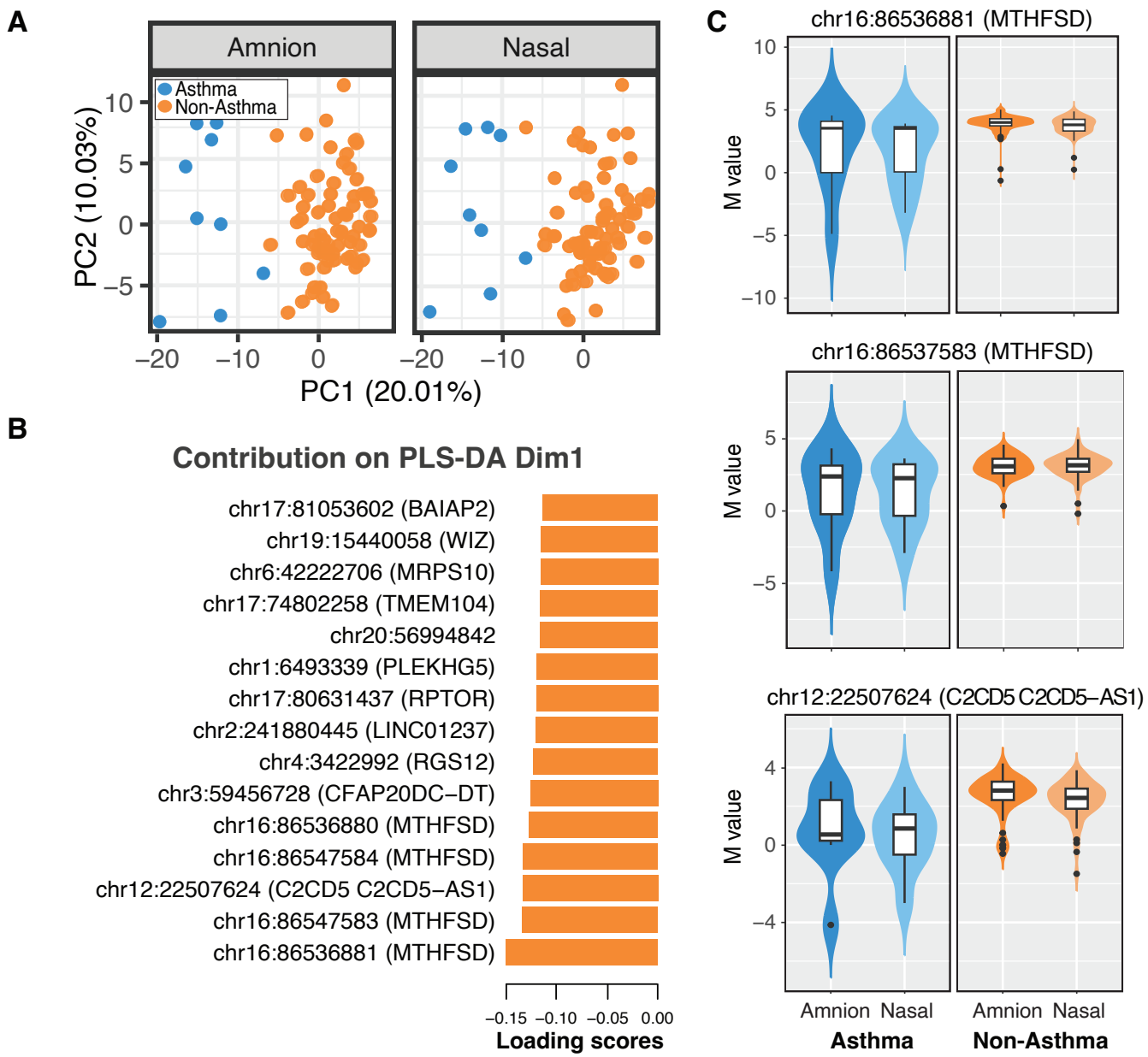
A
Amnion
Nasal
Asthma
Non-Asthma
PC2 (10.03%)
PC1 (20.01%)
B
Contribution on PLS-DA Dim1
chr17:81053602 (BAIAP2)
chr19:15440058 (WIZ)
chr6:42222706 (MRPS10)
chr17:74802258 (TMEM104)
chr20:56994842
chr1:6493339 (PLEKHG5)
chr17:80631437 (RPTOR)
chr2:241880445 (LINC01237)
chr4:3422992 (RGS12)
chr3:59456728 (CFAP20DC−DT)
chr16:86536880 (MTHFSD)
chr16:86547584 (MTHFSD)
chr12:22507624 (C2CD5 C2CD5−AS1)
chr16:86547583 (MTHFSD)
chr16:86536881 (MTHFSD)
Loading scores
C
chr16:86536881 (MTHFSD)
chr16:86537583 (MTHFSD)
chr12:22507624 (C2CD5 C2CD5−AS1)
M value
Amnion Nasal
Asthma
Non-Asthma

666

667 **Figure 4. Methylation changes associated with maternal asthma in the conserved signature.** (A) Principal Component Analysis
668 (PCA) of DNA methylation variation in newborn amnion and nasal tissues, showing the first two principal components (PC1 and PC2).
669 Samples are coloured based on maternal asthma history, with asthma in orange and non-asthma in blue. (B) Bar plot of loading scores
670 from Dimension 1 (Dim1) of a Partial Least Squares Discriminant Analysis (PLS-DA), highlighting the top 15 differentially methylated
671 CpG sites associated with maternal asthma. (C) Violin plots of the top three CpG sites identified by PLS-DA, showing the distribution
672 of methylation levels (expressed as M-values) at features associated with maternal asthma in newborn amnion and nasal tissues, further
673 stratified by maternal asthma history during pregnancy status.

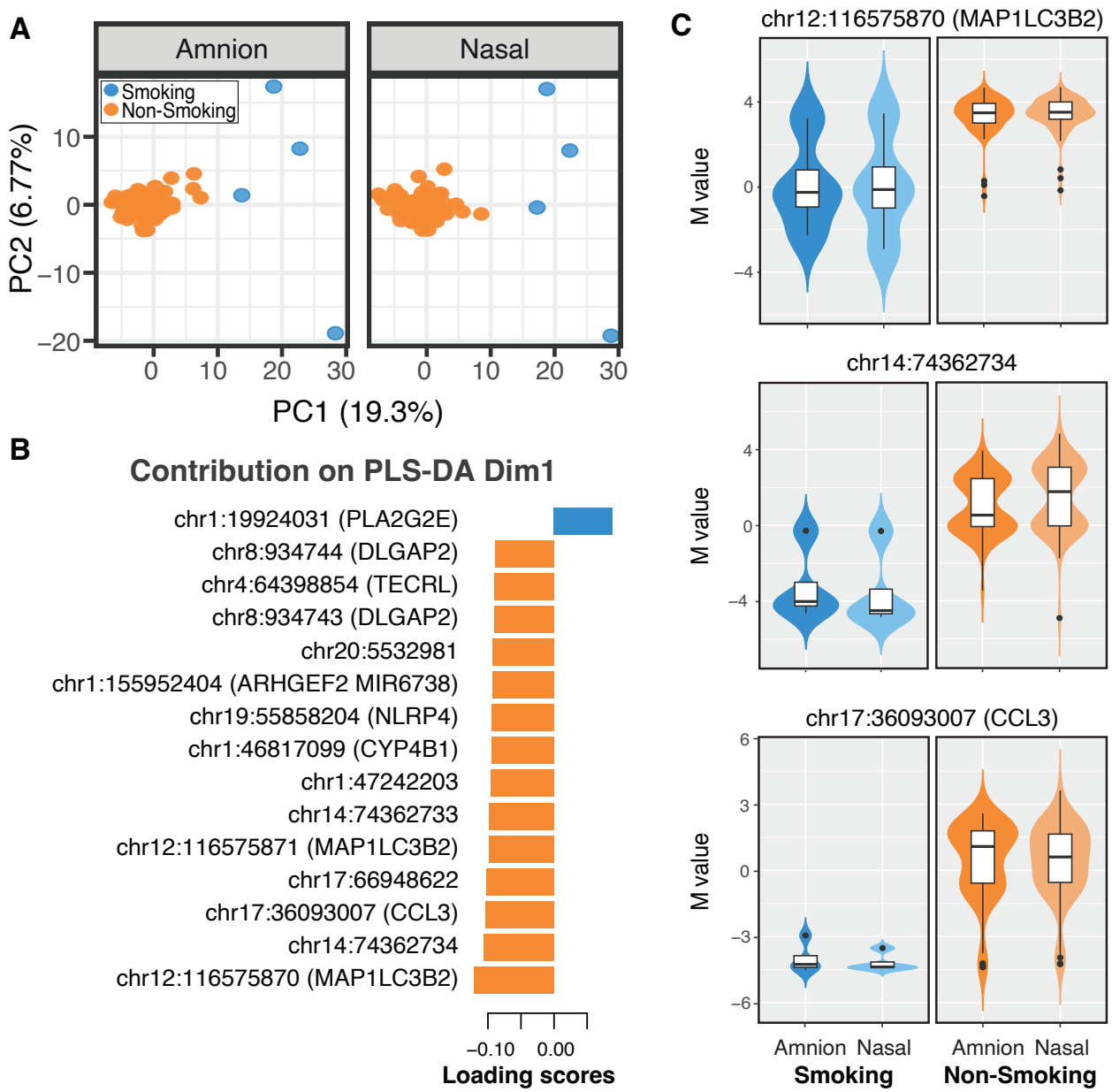
A
Amnion
Nasal
Smoking
Non-Smoking
PC2 (6.77%)
PC1 (19.3%)
B
Contribution on PLS-DA Dim1
chr1:19924031 (PLA2G2E)
chr8:934744 (DLGAP2)
chr4:64398854 (TECRL)
chr8:934743 (DLGAP2)
chr20:5532981
chr1:155952404 (ARHGEF2 MIR6738)
chr19:55858204 (NLRP4)
chr1:46817099 (CYP4B1)
chr1:47242203
chr14:74362733
chr12:116575871 (MAP1LC3B2)
chr17:66948622
chr17:36093007 (CCL3)
chr14:74362734
chr12:116575870 (MAP1LC3B2)
Loading scores
C
chr12:116575870 (MAP1LC3B2)
chr14:74362734
chr17:36093007 (CCL3)
M value
Amnion Nasal
Smoking
Non-Smoking

675 **Figure 5. Methylation changes associated with maternal smoking exposure in the conserved signature.** (A) Principal Component
676 Analysis (PCA) of DNA methylation variation in newborn amnion and nasal tissues, showing the first two principal components (PC1
677 and PC2). Samples are coloured based on maternal smoking exposure, with smoking exposure in orange and non-smoking exposure in
678 blue. (B) Bar plot of loading scores from Dimension 1 (Dim1) of a Partial Least Squares Discriminant Analysis (PLS-DA), highlighting
679 the top 15 differentially methylated CpG sites associated with maternal smoking exposure. (C) Violin plots of the top three CpG sites
680 identified by PLS-DA, showing the distribution of methylation levels (expressed as M-values) at features associated with maternal
681 smoking exposure in newborn amnion and nasal tissues, further stratified by prenatal smoking status.

682
683